Electronic Supporting information

Enhancement of Photocatalytic CO_2 Reduction in BiOBr through Chirality-induced Electron Spin Polarization Regulation

Yong Pu [a], Tianyue Wang [a], Chang Lin [a], Dun Wang [a], Zhongxin Liu [a], Yue Tian [b,*], Jieqiong Wang [b,*]

a. Department of School of Chemical Engineering and Technology, Hainan University, Haikou, China.
b. School of Marine Science and Engineering, Hainan University, Haikou, China.

Corresponding author: Y. Tian (tianyue@hainanu.edu.cn),
J. Q. Wang (wangjq@hainanu.edu.cn).

Experimental Section

1. Materials.

Bismuth nitrate pentahydrate (99%) and sodium bromide (99%) were procured from Aladdin Reagents Co., Ltd. Ethylene glycol (98%), sodium hydroxide (97%), and D/L-sorbitol (97%) were sourced from Shanghai Macklin Biochemical Co., Ltd. Ethyl alcohol (99.7%) and acetone (99.5%) were obtained from Xilong Chemical Co., Ltd. Deionized water with a resistivity of approximately 18.2 MΩ·cm was acquired using a Milli-Q synthesis system. All chemicals were utilized without further purification, and all solutions were prepared with deionized water.

2. Preparation of chiral BiOBr.

The fluorine-doped tin oxide (FTO) substrates (20 × 10 × 1.6 mm, coating thickness = 250 nm, sheet resistance ≤ 14 Ω) were thoroughly cleaned by immersion in acetone, ethanol, and deionized water for 15 minutes each in an ultrasonic bath. Subsequently, the substrates were soaked in a 1 mM $Bi(NO_3)_3•5H_2O$ nitric acid solution for 24 hours. To prepare the chiral inducer, 1.3 mmol of D/L-sorbitol (D/L-Sor) was dissolved in a mixed solution of 10 mL of deionized water and 40 mL of ethylene glycol (EG) and stirred continuously for 20 minutes. Following this, 1.3 mmol of $Bi(NO_3)_3•5H_2O$ was added to achieve a homogeneous solution. After an additional 20 minutes of stirring, 1.3 mmol of NaBr and 190 μL of NaOH (0.1 M) were added sequentially to the mixture. The resulting solution, along with the activated FTO substrate, was subsequently transferred to a 100 mL Teflon-lined autoclave and subjected to hydrothermal treatment at 140 °C for 24 hours.

3. Photocatalytic reduction CO_2.

Photocatalytic carbon dioxide reduction was conducted in a top-irradiated Pyrex cylindrical vessel without the use of sacrificial reagents during the reaction. Typically, 0.01 g of the photocatalyst was uniformly deposited onto a glass substrate (2 × 2 cm) and placed inside the reactor. Concurrently, 500 mg of potassium bicarbonate ($KHCO_3$) was added to the bottom of the reactor, ensuring it did not contact the glass substrate. After evacuating the reactor using a vacuum pump, a carbon dioxide and water vapor atmosphere was created by injecting 1 mL of 6 M hydrochloric acid (HCl) into the reactor with a gas-tight syringe. Once adsorption equilibrium was achieved, the reactor was irradiated with a xenon lamp (λ ≥ 420 nm, HSX-F300, NBeT) at a fixed temperature of 25 °C, assisted by circulating cooling water. Based on this methodology, we

investigated the effect of different polarized light sources on the catalytic properties of the chiral materials. To facilitate this, polarizers (right- and left-handed) were positioned between the light source outlet and the opening of the reaction vessel. The gaseous products were analyzed using an Agilent 8890 gas chromatography (GC) system equipped with a flame ionization detector (FID) and a thermal conductivity detector (TCD), via manual injection with a gas-tight syringe (SGE syringe, TRAJAN, 500 μL).

4. Catalyst characterization.

X-ray diffraction (XRD) patterns were recorded using a Bruker D8 diffractometer over a scanning angle range of 10° to 80°, employing Cu Kα radiation as the source. X-ray photoemission spectroscopy (XPS) was performed with a Thermo Scientific K-Alpha system. The BiOBr microstructure was examined using transmission electron microscopy (TEM, FEI Talos F200s) and field-emission scanning electron microscopy (SEM, Thermo Scientific G4 UC). Fourier-transform infrared spectroscopy (FTIR) spectra were analyzed using a Thermo Nicolet iS50 spectrometer. The optical absorption properties of the synthesized materials were assessed with a UV–vis spectrophotometer (Shimadzu UV-2600i). Photoluminescence (PL) spectra were acquired on an FLS1000 system with an excitation wavelength of 255 nm. In situ FTIR spectra were recorded during the photoreduction of CO_2. Circular dichroism (CD) spectra were obtained using a JASCO J-1500 spectropolarimeter. GC-MS measurements were performed on Agilent 7890B-5977B.

5. Photoelectrochemical measurements.

Photocurrent measurements and electrochemical impedance spectroscopy (EIS) were conducted using a conventional three-electrode setup on an electrochemical workstation (CS350M). Typically, a 5 mg sample was dispersed in a 1:1 mixture of 300 μL water and 300 μL ethanol. The suspension was prepared by sonicating the mixture for 10 minutes. The FTO conducting glass (1.1×10×20 mm) was coated with 200 μL of the suspension and used as the working electrode. An Ag/AgCl electrode and a platinum wire were used as the reference and counter electrodes, respectively. A 0.5 M sodium sulfate aqueous solution was used as the electrolyte.

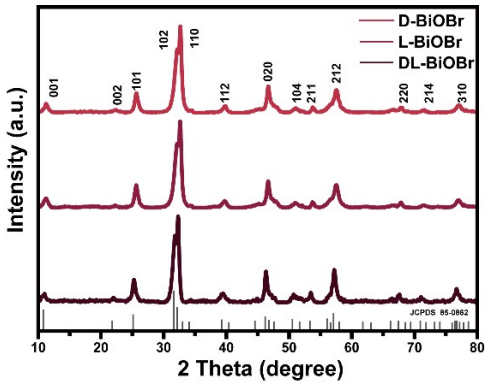

Figure S1. XRD patterns of D-, L- and DL-BiOBr.

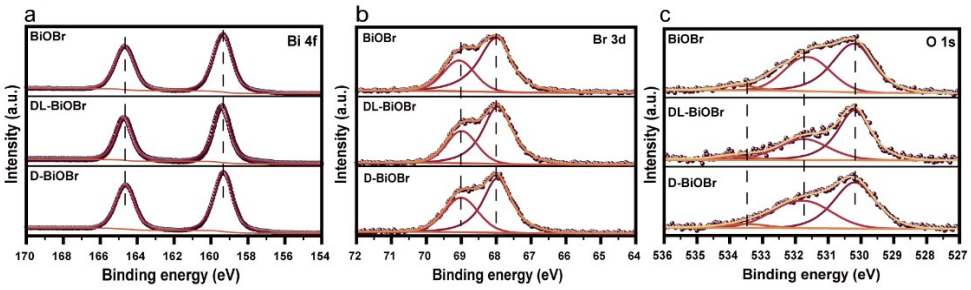

Figure S2. High-resolution XPS fine spectra of BiOBr, DL-BiOBr, and D-BiOBr. (a) Bi 4f, (b) Br 3d and (c) O 1s.

The Bi 4f XPS fine spectra exhibit two distinct peaks at 159.37 eV and 164.67 eV, which are attributed to the Bi $4f_{7/2}$ and Bi $4f_{5/2}$ levels, respectively[1]. The Br 3d spectra displays closely spaced spin-orbit components, with peak values centered at approximately 67.99 eV for Br $3d_{5/2}$ and 69.07 eV for Br $3d_{3/2}$, respectively[2]. In the O 1s XPS spectra, three peaks are at 530.21 eV, 531.71 eV, and 533.47 eV, corresponding to lattice oxygen (Bi-O), chemisorbed oxygen (oxygen vacancies, O_{Vs}), and hydroxyl groups (O-H), respectively[3].

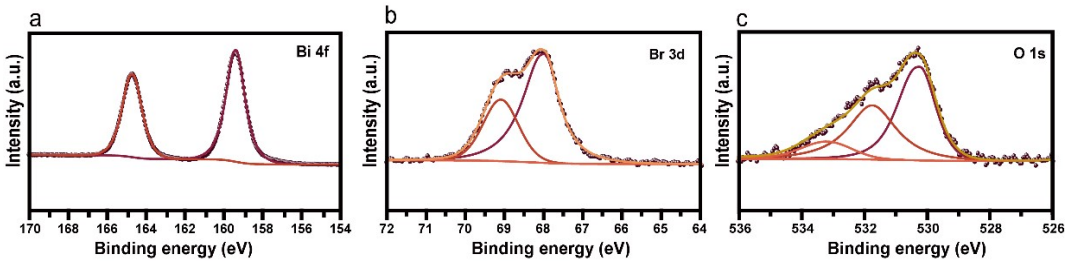

Figure S3. XPS fine spectra of L-BiOBr. (a) Bi 4f, (b) Br 3d and (c) O 1s.

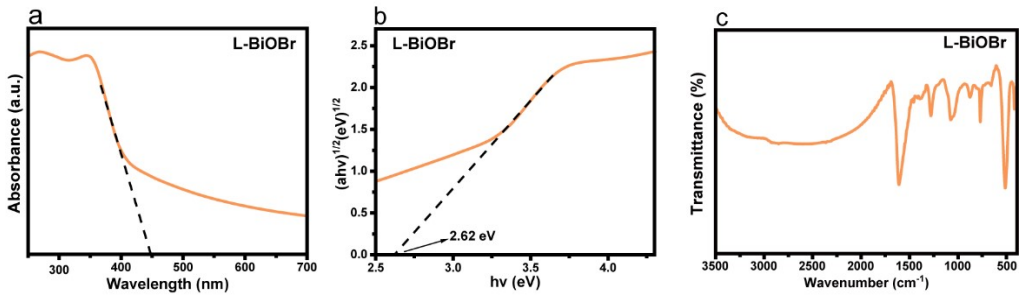

Figure S4. UV absorption spectrum (a) of L-BiOBr and the corresponding Tauc plots (b) using $(F(R)hv)^2$ as a function versus the photon energy band gap plots. (c) FTIR spectrum of L-BiOBr.

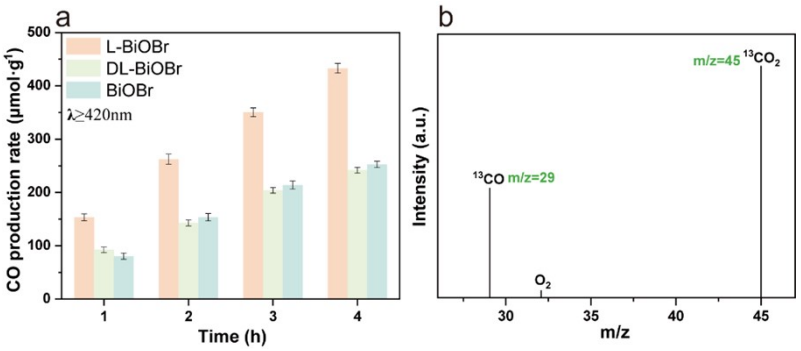

Figure S5. (a) Photocatalytic performance of L-BiOBr, DL-BiOBr and BiOBr under natural light. (b) GC-MS analysis for photocatalytic product over D-BiOBr using $^{13}CO_2$ as carbon resource.

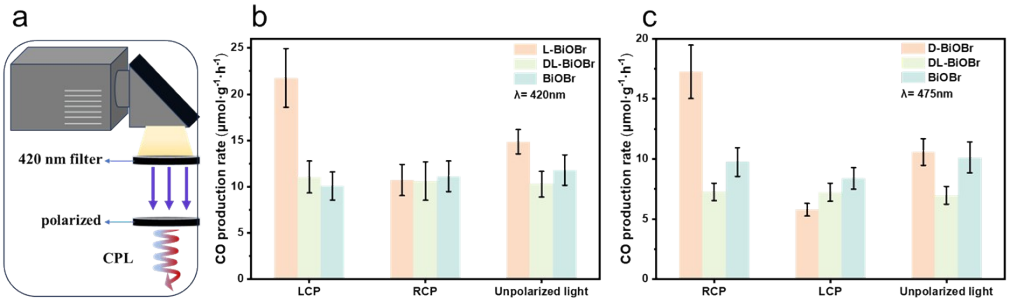

Figure S6. (a) Schematic diagram of the device for converting monochromatic light into circularly polarized light. (b) Time course for photocatalytic CO_2 reduction over D-BiOBr using circularly polarized light with wavelengths of 420 (b) and 475nm (c) as excitation.

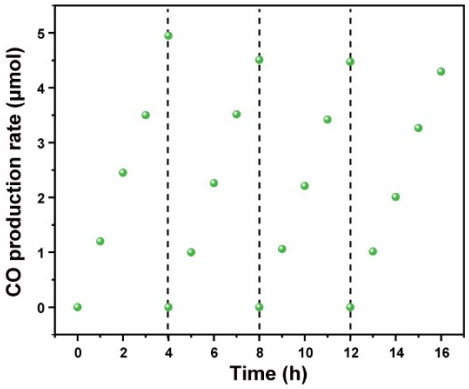

Figure S7. Recycling stability test of photocatalytic CO_2 reduction over D-BiOBr.

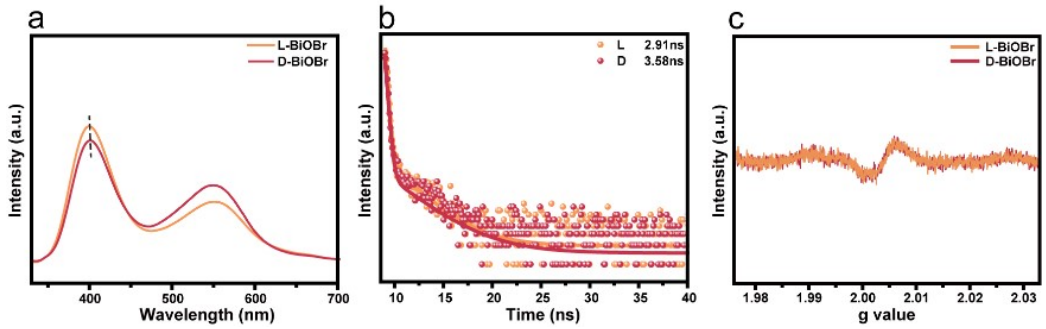

Figure S8. (a, b) PL spectra and nanosecond time-resolved PL decay curves of L- and D-BiOB. (c) EPR spectra of L- and D-BiOBr.

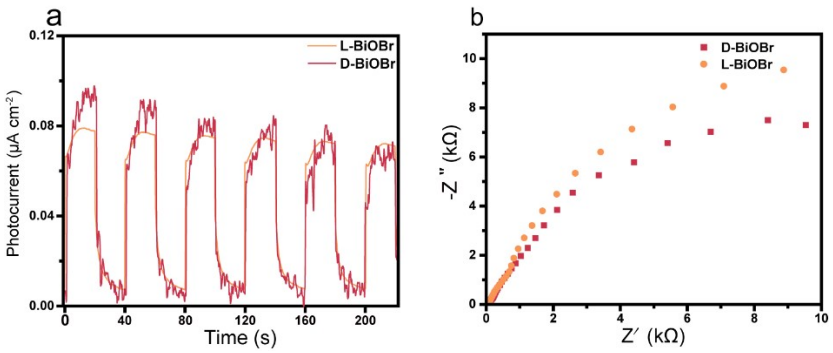

Figure S9. Photocurrent and EIS plots for L- and D-BiOBr.

Table S1. Comparison of photocatalytic CO_2 reduction performance over D-/L-BiOBr and BiOBr-based photocatalysts.

photocatalyst	Light Source	Maximum CO production (μ mol g^{-1} h^{-1})	Ref.
D-BiOBr	300W Xe lamp (λ≥420nm)	109	This work
L-BiOBr	300W Xe lamp (λ≥420nm)	98	This work
V_{Bi}-BiOBr	300W Xe lamp	20.1	5
$BiOBr_XCl_{1-X}$	300W Xe lamp	15.86	6
BiOBr	300W Xe lamp	87.4	7
P/Bi-BiOBr	300W Xe lamp (λ=400 nm)	58.40	8
BiOBr	300 W Xe lamp	21.6	9
BiOBr/ACSs	300 W Xe lamp	23.74	10
Bi-BiOBr	300 W Xe lamp	11.45	11
BiOBr/TCN	300 W Xe lamp	10.89	12
$BiOBr/NH_2$-UiO-66	300 W Xe lamp	9.19	13
BiOBr/CdS	300 W Xe lamp	13.6	14
Au_{25}NCs/BiOBr	300 W Xe lamp	43.57	15
NH_2/BOB-OH	300 W Xe lamp	35.8	16
BiOBr	300 W Xe lamp	71.23	17
BiOBr-mof	300 W Xe lamp	47.17	18

References

1. X. Jin, C. Lv, X. Zhou, H. Xie, S. Sun, Y. Liu, Q. Meng and G. Chen, *Nano Energy*, 2019, **64**, 103955.
2. J. Di, J. Xia, M. Ji, S. Yin, H. Li, H. Xu, Q. Zhang and H. Li, *J. Mater. Chem. A*, 2015, **3**, 15108–15118.
3. P. Li, Z. Zhou, Q. Wang, M. Guo, S. Chen, J. Low, R. Long, W. Liu, P. Ding, Y. Wu and Y. Xiong, *J. Am. Chem. Soc*., 2020, **142**, 12430–12439.
4. H. Wang, Z. Chen, Y. Shang, C. Lv, X. Zhang, F. Li, Q. Huang, X. Liu, W. Liu, L. Zhao, L. Ye, H. Xie and X. Jin, *ACS Catal*., 2024, **14**, 5779–5787.
5. J. Di, C. Chen, C. Zhu, P. Song, J. Xiong, M. Ji, J. Zhou, Q. Fu, M. Xu, W. Hao, J. Xia, S. Li, H. Li and Z. Liu, *ACS Appl. Mater. Inter*., 2019, **11**, 30786–30792.
6. M. Gao, J. Yang, T. Sun, Z. Zhang, D. Zhang, H. Huang, H. Lin, Y. Fang and X. Wang, *Appl. Catal. B*, 2019, **243**, 734–740.
7. J. Wu, X. Li, W. Shi, P. Ling, Y. Sun, X. Jiao, S. Gao, L. Liang, J. Xu, W. Yan, C. Wang and Y. Xie, *Angew. Chem. Int. Ed*., 2018, **57**, 8719–8723.
8. J. Zhu, Y. Li, X. Wang, J. Zhao, Y. Wu and F. Li, *ACS Sustain. Chem. Eng.*, 2019, **7**, 14953–14961.
9. X. Ren, M. Gao, Y. Zhang, Z. Zhang, X. Cao, B. Wang and X. Wang, *Appl. Catal. B*, 2020, **274**, 119063.
10. K. Liu, X. Zhang, C. Zhang, G. Ren, Z. Zheng, Z. Lv and C. Fan, *RSC. Adv*., 2019, **9**, 14391–14399.
11. Z. Fan, Y. Wu, Y. Luo, Y. Qin, Y. Xie, Y. Ling and Y. Wang, *Sep. Purif. Technol*., 2025, **352**, 128230.
12. W. Tao, Q. Tang, J. Hu, Z. Wang, B. Jiang, Y. Xiao, R. Song and S. Guo, *J. Mater. Chem. A*, 2023, **11**, 24999–25007.
13. J. Liu, W. Qin, Y. Wang, Q. Xu, Y. Xie, Y. Chen, Y. Dai and W. Zhang, *Sep. Purif. Technol*., 2024, **344**, 127289.
14. Q. Yang, W. Qin, Y. Xie, K. Zong, Y. Guo, Z. Song, G. Luo, W. Raza, A. Hussain, Y. Ling, J. Luo, W. Zhang, H. Ye and J. Zhao, *Sep. Purif. Technol*., 2022, **298**, 121603.
15. J. Tian, K. Zhong, X. Zhu, J. Yang, Z. Mo, J. Liu, J. Dai, Y. She, Y. Song, H. Li and H. Xu, *Chem. Eng. J*., 2023, **451**, 138392.
16. X. Li, J. Cao, X. Jia, S. Li, X. Jin, Q. Wang, S. Chen and H. Lin, *Appl. Catal. B*, 2025, **362**, 124713.
17. J. Xie, Z. Lu, Y. Feng, J. Huang, J. Hu, A. Hao and Y. Cao, *Nano Res*., 2024, **17**, 297–306.
18. X. Yue, L. Cheng, F. Li, J. Fan and Q. Xiang, *Angew. Chem. Int. Ed*., 2022, **61**, e202208414.